

Scalable Quantum Error Correction for Surface Codes using FPGA

Namitha Liyanage, Yue Wu, Alexander Deters and Lin Zhong
Department of Computer Science, Yale University, New Haven, CT

Abstract

A fault-tolerant quantum computer must decode and correct errors faster than they appear. The faster errors can be corrected, the more time the computer can do useful work. The Union-Find (UF) decoder is promising with an average time complexity slightly higher than $O(d^3)$. We report a distributed version of the UF decoder that exploits parallel computing resources for further speedup. Using an FPGA-based implementation, we empirically show that this distributed UF decoder has a sublinear average time complexity with regard to d , given $O(d^3)$ parallel computing resources. The decoding time per measurement round decreases as d increases, a first time for a quantum error decoder. The implementation employs a scalable architecture called Helios that organizes parallel computing resources into a hybrid tree-grid structure. Using Xilinx’s cycle-accurate simulator, we present cycle-accurate decoding time for d up to 15, with the phenomenological noise model with $p = 0.1\%$. We are able to implement d up to 7 with a Xilinx ZC106 FPGA, for which an average decoding time is 120 ns per measurement round. Since the decoding time per measurement round of Helios decreases with d , Helios can decode a surface code of arbitrarily large d without a growing backlog.

1 Introduction

The high error rates of quantum devices pose a significant obstacle to the realization of a practical quantum computer. As a result, the development of effective quantum error correction (QEC) mechanisms is crucial for the successful implementation of a fault-tolerant quantum computer.

One promising approach for implementing QEC is the use of surface codes [1–3] in which information of a single qubit (called a logical qubit) is redundantly encoded across many physical data qubits, with a set of ancillary qubits interacting with the data qubits. By periodically measuring the ancillary qubits, one can detect and potentially correct errors in physical qubits.

Once the presence of errors has been detected through the measurement of ancillary qubits, a classical algorithm, or decoder, guesses the underlying error pattern based on the measurement results. The faster errors can be corrected, the more time a quantum computer can spend on useful work. Due to the error rate of the state of the art qubits, very large surface codes ($d > 25$) are necessary to achieve fault-tolerant quantum computing [2, 4, 5]. See §2 for more background.

As surveyed in §3, previously reported decoders capable of decoding errors as fast as measured, or backlog-free, either exploit limited parallelism [6, 7], or sacrifice accuracy [8, 9]. The largest d reported for any backlog-free implementations is 5 [6], based on a design that is physically infeasible beyond $d = 5$.

In this paper we report a *distributed Union-Find (UF) decoder* (§4) and its FPGA implementation called *Helios* (§5). Given $O(d^3)$ parallel resources, our decoder achieves sublinear average time complexity according to empirical results for d up to 15, the first to the best of our knowledge. Notably, adding more parallel resources will not reduce the time complexity of the decoder, due to the inherent nature of error patterns. Our decoder is a distributed design of and logically equivalent to the UF decoder first proposed in [10]. We implement the distributed UF decoder with Helios, a scalable architecture for organizing the parallel computation units. Helios is the first architecture of its kind that can scale to arbitrarily large surface codes by exploiting parallelism at the vertex level of the model graph. In §6, we report experimental validations of the distributed UF decoder and Helios with a ZCU106 FPGA board [11] which is capable of running surface codes up to $d = 7$. For $d = 7$ the decoder has an average decoding time of 120 ns per measurement round, faster than any existing decoder. We validate our design for surface codes of $d > 7$ by using Xilinx Vivado cycle accurate simulator [12]. These validations successfully demonstrate, for the first time, a decoder design with decreasing average time per measurement round when d increases. This shows evidence that the decoder can scale to arbitrarily large surface codes without a growing backlog.

2 Background

2.1 Qubit and Errors

Qubit is the basic unit of quantum computing which is represented as $|\psi\rangle = \alpha|0\rangle + \beta|1\rangle$. Here α and β are complex numbers such that $|\alpha|^2 + |\beta|^2 = 1$ and $|0\rangle$ and $|1\rangle$ are the basis states of a qubit.

Unlike classical bits, qubits are highly susceptible to errors. A qubit can unintentionally interact with its surrounding resulting in a change of its quantum state. Even the latest quantum computers still have an error rate of 10^{-3} [4] which is significantly worse than classical computers which have error rates lower than 10^{-18} . In contrast a useful quantum application requires an error rate of 10^{-15} or below necessitating error correction. Errors in qubits can be modeled as bit flip errors and phase flip errors. A bit flip is marked by the X operator, i.e., $X|\psi\rangle = \beta|0\rangle + \alpha|1\rangle$, while a phase flip is marked by Z operator, i.e., $Z|\psi\rangle = \alpha|0\rangle - \beta|1\rangle$.

2.2 Error Correction and Surface Code

Quantum Error Correction (QEC) is more challenging than classical error correction due to the nature of Quantum bits. First, qubits cannot be copied to achieve redundancy due to the no-cloning theorem. Second, the value of the qubits cannot be directly measured as measurements perturb the state of qubits. Therefore QEC is achieved by encoding the *logical state* of a qubit, as a highly entangled state of many physical qubits. Such an encoded qubit is called a *logical qubit*.

The surface code is the widely used error correction code for quantum computing due to its high error correction capability and the ease of implementation due to only requiring connectivity between adjacent qubits. A distance d surface code is a topological code made out of a $(2d - 1) \times (2d - 1)$ array of qubits as shown in Figure 1. A key feature of surface codes is that a larger d can exponentially reduce the rate of logical errors making them advantageous. For example, even if the physical error rate is 10 times below the threshold, d should be greater than 17 to achieve a logical error rate below 10^{-10} [2].

A surface code contains two types of qubits, namely data qubits and ancilla qubits. The data qubits collectively encode the *logical state* of the qubit. The ancilla qubits (called X-type and Z-type) entangle with the data qubits and by periodically measuring the ancilla qubits, physical errors in all qubits can be discovered and corrected. An X error occurring in a data qubit will flip the measurement outcome of Z ancilla qubits connected with the data qubit and Z error will flip the X ancilla qubits likewise. Such a measurement outcome is called *non-trivial measurement value*. Because ancilla qubits themselves could also suffer from physical qubit errors, multiple rounds of measurements are necessary. Figure 2 shows some example physical qubit errors occurring in a surface code and how

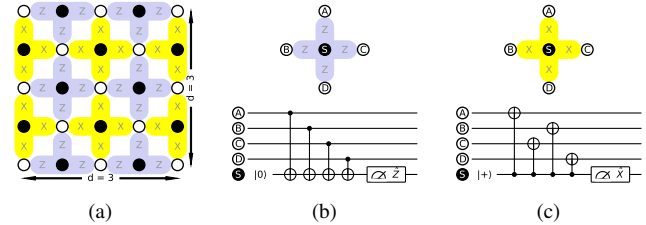


Figure 1: (a) : CSS surface code ($d = 3$), a commonly used type of surface code. The white circles are data qubits and the black the Z-type and X-type ancillas. (b) and (c) : Measurement circuit of Z-type and X-type ancillas. Excluding the ancillas in the border, each Z-type and X-type ancilla interacts with 4 adjacent data qubits.

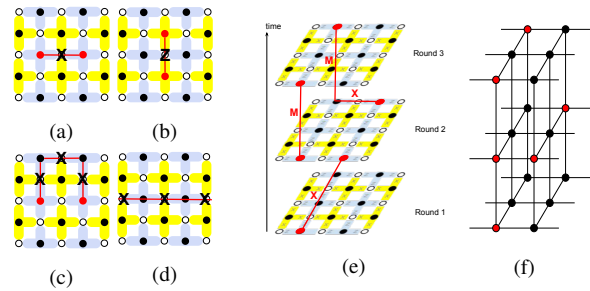


Figure 2: (a) to (d) : Various error patterns on $d = 3$ surface code. X and Z mark the corresponding physical qubit errors. Ancillas reporting non trivial measurements are shown in red. The red lines are to visualize error chains. (a) isolated X error (b) isolated Z error (c) error chain of three X errors (d) error chain introducing a logical error which has no non-trivial measurements. Note that even though (a) and (c) are different error patterns, they produce the same syndrome. (e) Error patterns spread across multiple measurement rounds. Here single X and Z errors can also spread across two rounds and error chains can include measurement errors (indicated by 'M') as well. (f) Decoding graph with vertices with nontrivial measurement marked red for the error pattern in (e).

they are detected by ancilla qubits. We show X and Z errors separately because they can be independently dealt with in the same way. The outcomes from these multiple rounds of measurements of ancilla qubits constitute a *syndrome*.

A syndrome can be conveniently represented by a graph called *decoding graph* in which a vertex represents a measurement outcome of an ancilla and an edge a data qubit. Vertices of nontrivial measurement outcome are specially marked. The weight of edge is determined by the probability of error in the corresponding data qubit or measurement. For distance d surface code, there are $d \times (d - 1)$ vertices. This decoding graph can be extended to three dimensional in which multiple identical planar layers are stacked on each other. Each layer represents a round of measurement. The total number of rounds is usually the same as the distance of the surface code. Corresponding vertices in adjacent layers are connected by edges which represent the probability of measurement error of the corresponding ancilla. That is, there are $d \times d \times (d - 1)$ vertices in this three-dimensional graph. Figure 2f shows the decoding graph for a syndrome from $d = 3$ surface code.

2.3 Error Decoders

Given a syndrome, an error decoder identifies the underlying error pattern, which will be used to generate a correction pattern. As multiple error patterns can generate the same syndrome, the decoder has to make a probabilistic guess of the underlying physical error. The objective is that when the correction pattern is applied, the chance of the surface code entering a different logical state (i.e a logical error) will be minimized.

Metrics The two important aspects of decoders are accuracy and speed. A decoder must correct errors faster than syndromes are produced to avoid a backlog. A faster decoder also allows more time for the quantum hardware to do actual useful work. The average decoding time per measurement round is a widely used criteria for speed.

A decoder must make careful tradeoff between speed and accuracy. A faster decoder with lower accuracy requires a larger d to achieve any given logical error rate, which may require more computation overall.

Union-Find (UF) Decoder The UF decoder is a fast surface code decoder design first described by Delfosse and Nickerson [10]. According to [13], it can be viewed as an approximation to the blossom algorithm that solves minimum-weight perfect matching (MWPM) problems. It has a worst case time complexity of $O(d^3\alpha(d))$, where α is the inverse of Ackermann’s function, a slow growing function that is less than three for any practical code distances. Based on our analysis, it has an average case time complexity slightly higher than $O(d^3)$.

algorithm 1 describes the UF decoder. It takes a decoding graph $\mathcal{G}(\mathbf{V}, \mathbf{E})$ as input. Each edge $e \in \mathbf{E}$ has a weight and a growth, denoted by $e.w$ and $e.g$, respectively. $e.g$ is initialized with 0 and the decoder may grow $e.g$ until it reaches $e.w$. When that happens, we say the edge is *fully grown*.

The decoder maintains a set of odd clusters, denoted by \mathcal{L} . \mathcal{L} is initialized to include all $\{v\}$ that $v \in \mathbf{V}$ is non-trivial (L81). Each cluster C keeps track of whether its cardinality is odd or even as well as its root element.

The UF decoder iterates over growing and merging the odd cluster list until there are no more odd clusters (inside the **while** loop of **algorithm 1**). Each iteration has two stages: Growing and Merging. In the *Growing* stage, each odd cluster “grows” by increasing the *growth* of the edges incidental to its boundary. This process creates a set of *fully grown* edges \mathcal{F} (L86 to L95). The Growing stage is the more time-consuming step as it requires traversing all the edges in the boundary of all the odd clusters and updating the global edge table. Since the number of edges is $O(d^3)$, the UF decoder is not scalable for surface codes with large d .

In the *Merging* stage, the decoder goes through each fully-grown edge to merge the two clusters connected by the edge.

Algorithm 1: Union Find Decoder

```

input : A decoding graph  $\mathcal{G}(\mathbf{V}, \mathbf{E})$  with X (or Z) syndrome
output : A correction pattern
77 % Initialization
78 for each  $v \in \mathbf{V}$  do
79     if  $v$  is non-trivial then
80         Create a cluster  $\{v\}$ 
81     end
82 end
83 while there is an odd cluster do
84     % Growing
85      $\mathcal{F} \leftarrow \emptyset$ 
86     for each odd cluster  $C$  do
87         for each  $e = \langle u, v \rangle, u \in C, v \notin C$  do
88             if  $e.growth < e.w$  then
89                  $e.growth \leftarrow e.growth + 1$ 
90                 if  $e.growth = e.w$  then
91                      $\mathcal{F} \leftarrow \mathcal{F} \cup \{e\}$ 
92                 end
93             end
94         end
95     end
96     % Merging
97     for each  $e = \langle u, v \rangle \in \mathcal{F}$  do
98         UNION( $u, v$ )
99     end
100 end
101 Build correction within each cluster

```

When two clusters merge, the new cluster may become even.

When there is no more odd cluster, the decoder finds a correction within each cluster and combines them to produce the correction pattern (L101).

3 Related Work

There is a large body of literature on fast QEC decoding, e.g., [14–16]. The most related are solutions that leverage parallel compute resources.

Fowler [17] describes a method for decoding at the rate of measurement ($O(d)$). The proposed design divides the decoding graph among specialized hardware units arranged in a grid. Each unit contains a subset of vertices and can independently decode error chains contained within it. The design is based on the observation that large error patterns spanning multiple units are exponentially rare, so inter-unit communication is not frequently required. It, however, paradoxically assumes that the number of vertices per unit is “sufficient large” and a unit can find an MWPM for its vertices within half the measurement time on average. Not surprisingly, to date, no implementation or empirical data have been reported for this work. Our approach distributes computation to a vertex-level and leverages the same observation that communication between distant vertices is infrequent.

NISQ+[8] and QECOOL[9] parallelize computation at the ancilla level, where all vertices in the decoding graph representing measurements of one ancilla are handled by a single

compute unit. This results in an increase in decoding time per measurement round as d increases. In contrast we allocate a processing element per each vertex, which results in decreasing decoding time per measurement round with d at the expense of number of parallel units growing $O(d^3)$. Furthermore, they both implement the same greedy decoding algorithm that has much lower accuracy than the UF decoder used in this work. QECOOL has an accuracy that is approximately four orders of magnitude lower than that of a UF decoder [7] and NISQ+ ignores measurement errors further lowering its accuracy than QECOOL.

Skoric et al. [18] propose a method of using measurement round-level parallelism, in which a decoder waits for a large number of measurement rounds to be completed and then decodes multiple blocks of measurement rounds in parallel. By using sufficient parallel resources this method can achieve a rate of decoding faster than the rate of measurement. However, the latency of this approach grows with the number of measurement rounds the decoder needs to batch to achieve a throughput equal to the rate of measurement. In contrast, our approach exploits vertex-level parallelism and completes decoding of every d rounds of measurements with an average latency that grows sublinearly with d .

Pipelining can be considered a special form of using compute resources in parallel, i.e., in different pipeline stages. AFS [7] is a UF decoder architected in three pipeline stages. The authors estimate the decoder will have a 42 ns latency for $d = 11$ surface code, which is three times lower than what we report based on implementation and measurement. The authors assume a specialized hardware that is capable of running at 4 GHz and as a result, the decoding latency will be dominated by memory access. However, no implementation or cycle-accurate simulation is known for this decoder. Importantly, pipelining is limited in how much parallelism it can leverage: the number of pipeline stages. In contrast, parallelism of our decoder grows along d^3 , which enables us to achieve a sublinear average case latency.

LILLIPUT [6] is a three stage look-up-table based decoder similar to AFS. Look-up-table based decoders can achieve fast decoding but are not scalable beyond $d = 5$ as the size of the look-up table grows $O(2^{d^3})$. For $d = 7$ surface code with 7 measurement rounds, it would require a memory of 2^{168} Bytes, which is infeasible in any foreseeable future.

4 Distributed UF Decoder Design

Our goal to build a QEC decoder is scalability to the number of qubits. As surface codes can exponentially reduce logical error rate with respect to d , larger surface codes with hundreds or even thousands of qubits are necessary for fault-tolerant quantum computing. Therefore, the average decoding time per measurement round should not grow with d , to avoid exponential backlog for any larger d .

We choose the UF decoder for two reasons. First, it has much lower time complexity than the MWPM algorithm. Although in general the UF decoder achieve lower decoding accuracy than MWPM decoders, it is as accurate in many interesting surface codes and noise models [13]. Second, the UF decoder maintains much less intermediate states, which makes it easier to implement in a distributed manner. We observe that growing stage from L86 to L95 in [algorithm 1](#) operates on each vertex independently without dependencies from other vertices. A vertex requires only the parity of the cluster it is a part of for the growing stage. Second, during the merging stage, a vertex only needs to interact with its immediate neighbors (L98).

Like the original UF decoder, our distributed UF decoder is also based on the decoding graph. Logically, the distributed decoder associates a processing element (PE) with each vertex in the decoding graph. Therefore, When describing the distributed decoder, we often use PE and vertex in an interchangeable manner. PEs operate with the same algorithm, specified by [algorithm 2](#). The PE algorithm iterates over three stages.

4.1 PE States

A PE has direct read access to its local states and some states of incident PEs. A PE can only modify its local states.

Thanks to the decoding graph, a PE has immediate access to the following objects.

- v , the vertex it is associated with.
- $v.E$, the set of edges incident to v .
- $v.U$, the set of vertices that are incident to any $e \in v.E$. We say these vertices are adjacent to v .

The algorithm augments the data structures of vertex and edge of the decoding graph, according to the UF decoder design [10]. For each vertex $v \in V$, the following information is added

- id : a unique identity number which ranges from 1 to n where $n = |V|$. id is statically assigned and never changes.
- m is a binary indicating whether the measurement outcome is trivial (`false`) or not (`true`). m is initialized according to the syndrome.
- cid : a unique integer identifier for the cluster to which v belongs to, and is equal to the lowest id of all the vertices inside the cluster. The vertex with this lowest id is called the cluster root. $v.cid$ is initialized to be $v.id$. That is, each vertex starts with its own single-vertex cluster. When $cid = id$, the vertex is a root of a cluster.
- odd is a binary indicating whether the cluster is odd. odd is initialized to be m .
- $codd$ is a copy of odd .
- $stage$ indicates the stage the PE currently operates in

- `busy` is a binary indicating whether the PE has any pending operations.

For each edge $e \in E$, the decoder maintains $e.growth$, which indicates the growth of the edge, in addition to $e.w$, the weight. $e.growth$ is initialized as 0. The decoder grows $e.growth$ until it reaches $e.w$ and e becomes *fully grown*.

For clarity of exposition, we introduce a mathematical shorthand $v.nb$, the set of vertices connected with v by fully-grown edges, i.e., $v.nb = \{u | e = \langle v, u \rangle \in v.E \ \& \ e.growth = e.w\}$. We call these vertices the *neighbors* of v . Note neighbors are always adjacent but not all adjacent vertices are neighbors.

4.2 Shared memory based communication

We use coherent shared memory for shared state that has a single writer. For all shared memories, given the coherence, a read always returns the most recently written value. Like ordinary memory, we also assume both read and write are atomic.

- memory read/write for PE (v) and read-only for adjacent PEs, i.e., $\forall u \in v.U$. $v.cid$ and $v.odd$ reside in this memory (S1).
- memory read/write for PE (v) and read-only for the controller. The PE local states, $v.codd$, $v.stage$ and $v.busy$ reside in this memory (S2).
- memory for $e.growth$, which can be written by incident PEs (S3).
- memory read/write for the controller and read-only for all PEs. The controller state `global_stage` is stored in this memory (S4).

4.3 Message based communication

Only instance in our decoder where a PE needs to communicate with a distant PE is when a PE needs to notify the root when joining a new cluster (L32). Implementing this using shared memory is costly because the PE is not necessarily adjacent to the root. As there is one type of message in our decoder, each message M contains only the destination of the message. The destination take value from 1 to n , which represents the vertex identifier.

For the correctness of the decoder we only assume guaranteed delivery of messages and do not assume a time bound for message delivery.

4.4 PE Algorithm

All PEs iterate over three stages of operation. Within each stage, they operate independently but transit from one stage to the next when the controller updates `global_stage`. When a PE enters a stage, it sets $v.stage$ accordingly and keep $v.busy$

Algorithm 2: Algorithm for vertex v in the distributed UF decoder.

```

1  $v.cid \leftarrow v.id; v.odd \leftarrow v.m$ 
2 while true do
3   if global_stage = terminate then
4     return
5   end
6   growing(v)
7   merging(v)
8   syncing(v)
9 end

```

as `true` until it finishes all work in the stage. The controller uses these two pieces of information from all PEs to determine if a stage has started and completed, respectively (See §4.5).

We next describe the three stages of the PE algorithm. In the **Growing** stage, vertices at the boundary of an odd cluster increase $e.growth$ for boundary edges (L16). As PEs perform Growing simultaneously, two adjacent PEs may compare $e.w$ and $e.growth$ and update $e.growth$ for the same e . Such compare-and-update operations must be atomic to avoid data race.

In the **Merging** stage, two clusters connected through a fully-grown edge merge by adopting the lower cluster id (cid) of theirs. To achieve this each PE compares its cid with PEs connected through fully-grown edges (L31). If the other incident vertex of a fully grown edge has a lower cid the PE adopts the lower cid as its own (L31). Merging process continues until every PE in the cluster have the same cid which is the lowest $v.id$ of the cluster. This procedure is related to leader election in a distributed systems: vertices in a newly formed cluster must adopt the lowest id . The Merging stage also calculates the parity of the cluster. Each PE representing a non-trivial measurement (m is `true`) messages the root of the cluster it joins (L32). Likewise, the root updates its parity when it receives a message from a PE (L38).

In the **Syncing** stage, a root broadcasts its $v.odd$ to all PEs in its cluster, which is necessary for the next Growing stage. We achieve this using a modified version of the flooding algorithm, which uses shared memory instead of message passing. Every non-root node initially set its $v.odd$ as `false` and continues comparing $v.odd$ with PEs with fully connected edges. If any of the PEs connected with a fully grown edge has $v.odd$ as `true` the PE set its $v.odd$ as `true` (L53). If a cluster has $v.odd$ as `true` in the root, this results in propagating `true` to all vertices in the cluster similar to a flooding algorithm.

4.5 Controller Algorithm

The controller moves all PEs and itself along the three stages. In each stage, it checks for $v.busy$ signals and in addition in merging stage it checks for outstanding messages. The controller determines completion of a stage when all PEs have $v.busy$ as `false` and there are no outstanding messages.

Algorithm 3: Vertex growing algorithm

```
10 function growing(vertex v)
11   Wait until global_stage = growing
12   v.busy ← true; v.stage ← growing
13   if v.odd then
14     for each  $e = \langle u, v \rangle \in v.E$  atomic do
15       if  $e.growth < e.w$  and  $u.cid \neq v.cid$  then
16          $e.growth \leftarrow e.growth + 1$ 
17       end
18     end
19   end
20   v.busy ← false;
21 end
```

Algorithm 4: Vertex merging algorithm

```
22 function merging(vertex v)
23   Wait until global_stage = merging
24   v.busy ← true; v.stage ← merging
25
26   while true do
27     if global_stage ≠ merging then return
28
29     if  $\exists u \in v.nb$  s.t.  $u.cid < v.cid$  then
30       v.busy ← true
31       v.cid ←  $MIN(u.cid | u \in v.nb)$ 
32       if v.m then send M(v.cid)
33     else if  $\forall u \in v.nb, u.cid = v.cid$  then
34       v.busy ← false
35     end
36
37     for each received message M do
38       v.odd ←  $\neg v.odd$ 
39     end
40   end
41 end
```

Algorithm 5: Vertex syncing algorithm

```
42 function syncing(vertex v)
43   v.busy ← true; v.stage ← syncing
44   if v.cid ≠ v.id then v.odd ← false
45   v.codd ← v.odd
46
47   while true do
48     if global_stage ≠ syncing then return
49
50     if  $\forall u \in v.nb, u.odd = v.odd$  then
51       v.busy ← false
52     else
53       v.odd ← true
54       v.busy ← true
55     end
56   end
57 end
```

Upon completion, the controller updates the *global_stage* variable to move to the next stage and the PEs acknowledge this update by updating their own *v.stage* variable.

The controller also calculates the presence of odd clusters. At the end of the syncing stage, it reads the *v.odd* value of

Algorithm 6: The controller coordinates all PEs along stages and detects the presence of odd clusters.

```
58 while true do
59   global_stage ← growing
60   wait until  $\forall v \in V, v.stage = growing$ 
61   wait until  $\forall v \in V, v.busy = false$ 
62
63   global_stage ← merging
64   wait until  $\forall v \in V, v.stage = merging$ 
65   wait until  $\forall v \in V, v.busy = false$ 
66   wait until no outstanding messages in the system
67
68   global_stage ← syncing
69   wait until  $\forall v \in V, v.syncing = growing$ 
70   wait until  $\forall v \in V, v.busy = false$ 
71
72   if  $\forall v \in V, v.codd = false$  then
73     global_stage ← terminate
74     return
75   end
76 end
```

each vertex. If any vertex has *v.odd* = true, the controller updates the global stage variable to Growing to continue the algorithm. Otherwise, it updates it to Terminate to end the algorithm.

4.6 Time Complexity Analysis

The worst case time complexity of our distributed UF decoder is $O(d^3)$. The worst case occurs when parallelism is maximally lost in the system; all vertices are non-trivial and merge into a single cluster and the root must process all incoming messages from all other vertices (L38). However, the occurrence of the worst case scenario is extremely rare as larger clusters are exponentially unlikely to occur. Empirical results reported in §6 show that average time grows sublinearly with *d*.

The time complexity of the controller depends on the implementation of the shared memory for *v.busy* and checking for outstanding messages in the system. As both checks are logical OR operators of individual PE information, the most efficient implementation is a logical tree of OR operations which results in a time complexity of $O(\log(d))$. Thus, the overhead of coordination is significantly smaller than the worst case time complexity.

PE Communication Complexity The communication complexity of the shared memory based communication is $O(d^3)$. The leader election in the Merging stage and the broadcasting of *v.odd* in the Syncing stage are implemented using a shared memory based flooding algorithm. The time complexity of a flooding operation is $O(D)$, where *D* is the diameter of the cluster. Therefore, in the worst case the time complexity of flooding messages is $O(d^3)$.

The communication complexity of the message based communication is $O(d^6)$. Messages from each trivial measurement to the root of the cluster is proportional to the number of trivial vertices in the cluster and number of changes of cid of each vertex. Thus in the worst case there would be $O(d^6)$ messages and the time complexity will be $O(d^3)$.

5 Helios Architecture and Implementation

We next describe Helios, the architecture for the distributed UF decoder.

5.1 Overview

Helios organizes PEs and controller in a custom topology that combines a 3-D grid and a B+ tree as illustrated by [Figure 3](#) and explained below.

- PEs are organized according to the position of vertices they represent in the model graph. We assign $v.id$ sequentially, starting with 1 from bottom left corner and continuing in row-major order for each measurement round. Shared memory S1 ($v.cid$ and $v.odd$) and S2 ($v.codd$, $v.stage$, and $v.busy$) are added alongside each PE.
- Shared memory S3 ($e.growth$) is added to the incident PE with the lower id .
- A link between every two adjacent PEs to read from each other's S1 and for the one with the higher id to read the other's S4. This results in a network of links in a 3-D grid topology. As a PE represents a vertex in the model graph, a link represents an edge. Broad pink lines in [Figure 3](#) represent these links.
- A directional link between two adjacent PEs and between PEs with consecutive $v.id$ values for message passing (L32). These links are directed from the PE with higher $v.id$ to the other and are buffered. They are represented by blue arrows in [Figure 3](#).
- The controller, realized as a tree of control nodes (§5.3). The leaf control nodes of the tree contain shared memory S4.
- A link between each PE and the controller for the controller to read from S2 and for the PEs to read from S4. Dashed orange lines in [Figure 3](#) represent these links.

5.2 Message-passing between PEs

To implement the vertex merging algorithm ([algorithm 4](#)), a PE may send and receive messages from another PE, which is not necessarily adjacent. Helios implements this with the directional links and allows a PE to forward messages over directional links. The forward logic is trivially simple because

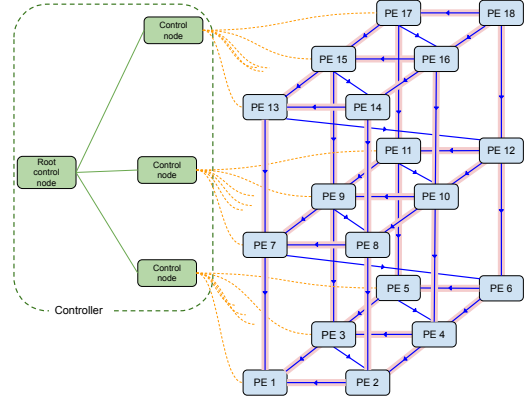


Figure 3: Helios architecture for $d=3$ surface code for 3 measurement rounds. As $d=3$ surface code has 6 (3 by 2) ancilla qubits, Helios contains of a $3 \times 2 \times 3$ PE array. PE n indicates PE with $v.id = n$.

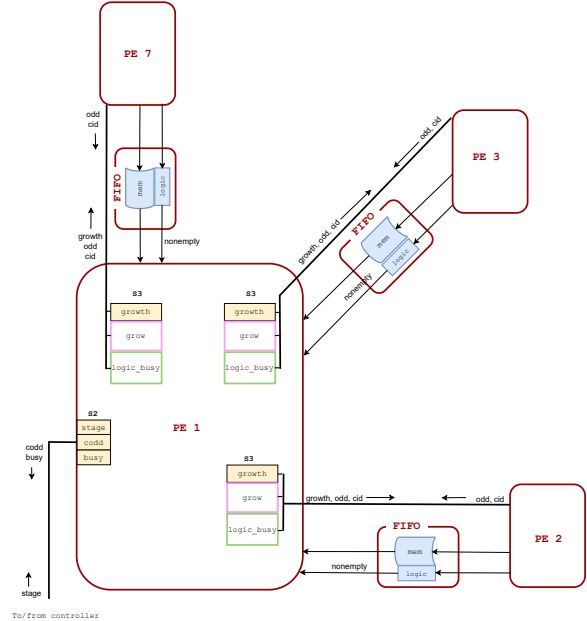


Figure 4: The bottom left corner of the PE array shown in [Figure 3](#). Only part of the logic and memory inside PE 1 is shown : growth (S3) is per edge and is stored in the PE with lower id . grow logic (in pink) calculates the updated growth value ([Figure 5](#)). logic_busy (in green) ([Figure 6](#)) is per adjacent PE and is used to calculate the busy signal.

- (1) a PE only messages another PE with a lower id per [algorithm 4](#) and (2) the links are directional from a PE with a higher id to that with a lower one.

We note that the directional links consist of the 3-D grid structure, from the edges of the model graph, and additional links between PEs with consecutive $v.id$ values, i.e., the “diagonal” ones in [Figure 3](#). The 3-D grid topology is optimal for exchanging messages between nearby PEs, which is frequent. The additional “diagonal” links prevent deadlocks by breaking potential circular dependency amongst several PEs, e.g., PE 1 to PE 4 in [Figure 3](#).

The directional links between PEs are buffered because a PE can receive multiple messages at a time. Because these buffers have a finite size, the sending PE can stall if a buffer is full. In §6.2, we show empirical evidence that stall rarely happens.

5.3 Controller

Helios implements the controller as a tree of nodes to avoid the scalability bottleneck. The controller requires four pieces of information from each PE: $v.codd$, $v.stage$, $v.busy$ and the presence of outstanding messages of the system. Each leaf node of the tree is directly connected with a subset of PEs. We can consider these PEs as the children of the leaf node. Each node in the tree gathers vertex information from its children and reports it to the parent. With information from all vertices, the root node runs [algorithm 6](#) and decides whether to advance the stage.

We leave height, branching factor and the subset of PEs connected to each leaf node as implementation choices. The necessary requirement is that the controller should not slow down the overall design.

5.4 FPGA Implementation

We next describe an implementation of Helios targeting a single FPGA. We choose FPGA for two reasons. It supports massively parallel logic, which is essential as the number of PEs grows proportional to d^3 in our distributed UF design. Moreover, it allows deterministic latency for each operation, which facilitates synchronizing all the PEs.

[Figure 4](#) shows a minimal diagram of a PE and a controller in the FPGA implementation.

Controller: Since we only use a single FPGA and evaluate with d below 20, a single node controller suffices.

Directional links: We implement the directional links as first-in-first-out (FIFO) buffers, which are mapped by Xilinx Vivado to LUT based RAMs. We choose the buffer size of four because our evaluations in §6.2 show that increasing the buffer size beyond four does not improve decoding time. Reducing the buffer size below four slightly increases decoding time (by 0.01%) while using the same number of LUTs as memory as a buffer of size four (up to 32).

Shared memory: We implement all shared memories as FPGA registers, i.e., `reg` in Verilog. FPGA registers by design guarantee that a read returns the last written value. In order to ensure that the S4 memory has a single writer, we modify the PE logic as shown in [Figure 5](#). Compare and update operation (L15) is implemented in the PE that the S3 memory resides in, and the PE increases $e.growth$ by two if both endpoints of the edge have $v.odd$ as true.

Detecting outstanding messages: Each PE updates its busy state based on pending messages in addition to conditions in L33 and L50 as shown in the code snippet in [Figure 6](#).

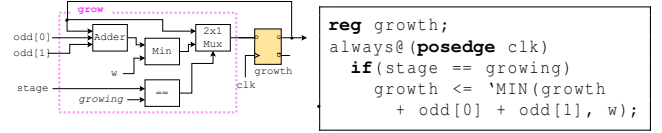


Figure 5: Circuit diagram of `grow` sub-module and Verilog implementation. This implements the atomic compare and update operation in L15 as part of the PE module. $odd[0]$ and $odd[1]$ represents the odd state of the two incident PEs of the edge.

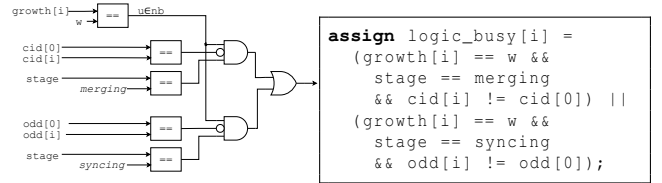


Figure 6: Circuit diagram of `logic_busy` sub-module and Verilog implementation. The sub-module is implemented per each adjacent PE which are indexed from 1 to the number of edges. The variables $odd[0]$ and $cid[0]$ represent the odd and cid of the PE, while $odd[i]$, $cid[i]$ and $growth[i]$ represent the corresponding values for the i^{th} adjacent PE and the edge connecting them.

The sub-circuit `logic_busy` checks for the conditions in L33 and L50 for each incident edge. In our FPGA implementation of FIFO buffers, when a value is written to a FIFO (using the `we` signal), `nonempty` state of the FIFO will be true in the next cycle. This results in at least one PE having `busy` as true when there are outstanding messages in the system. The controller reads `busy` every clock cycle to identify the completion of a stage.

In total, our implementation contains approximately 6000 lines of Verilog code. The code is available at [19].

On the ZCU106 FPGA development board [11], we are able to support the distributed UF decoder with d up to 7, due to resource limits. [Table 1](#) shows the resource usage for various d . While the numbers of vertices and edges grow by $O(d^3)$, the resource usage grows faster for the following reasons. First, resource usage by a PE grows due to the increase of bitwidth required for $v.id$, and $v.cid$. A PE for $d = 7$ with six adjacent PEs requires 182 LUTs and a similar PE for $d = 3$ requires only 127 LUTs. Second, PEs on the surface of the three-dimensional array as shown in [Figure 3](#) use less resources than those inside because the latter have more incident edges. When d increases a higher portion of PEs are inside the array.

We find that LUTs are the most critical resource in the FPGA for our design. It may be possible to run a design with $d = 15$ on a Xilinx VU19 FPGA [20], which currently has the highest number of LUTs among commercially available FPGAs at the time of this writing.

Existing commercial FPGAs like ZCU106 often dedicate a lot of silicon to digital signal processing (DSP) units and block RAMs (BRAMs). However, our design does not use

Table 1: Resource usage of Helios on ZCU106 FPGA board for various code distances

d	# of LUTs		# of registers
	as logic	as memory (FIFOs)	
3	2419	608	1187
5	18655	3236	7189
7	61793	12636	27664

any DSPs because it only requires comparison operators and fixed point additions. Our design does not use any BRAMs because the FIFOs have a depth of four and can be efficiently implemented using LUTs. Each BRAM tile in Xilinx has a default size of 18 Kbits and using BRAM for FIFOs would result in significant unused space in each BRAM tile. Therefore, an ideal FPGA designed to run our distributed UF decoder would be simpler than current large FPGAs, as it would only need a large number of LUTs, no DSP units and a limited amount of BRAM.

6 Evaluation

The main objective of our evaluation is to assess the scalability of our distributed UF implementation. To that end, we first describe our methodology and then show that the latency of our implementation grows sub-linearly with respect to the surface code size d .

6.1 Methodology

For speed, we measure the number of cycles required to decode a syndrome. To evaluate correctness, we compare the result of clustering generated by our distributed UF decoder with the clustering generated by the original UF decoder. We compare clusters because the original UF decoder and ours only differ in the clustering process. This shows that both decoders generate identical clusters in all cases tested, confirming the correctness of our decoder. In the rest of our evaluation, we will focus only on the speed of the distributed UF decoder and not on the accuracy of its results.

Experimental Setup We use two setups to evaluate our FPGA implementation. The primary setup is a Xilinx ZCU106 FPGA development board [11], which is capable of handling surface codes with d up to 7. As an alternative setup, we run our implementation on the Xilinx Vivado simulator [12], which emulates the behavior of FPGA in a cycle-accurate manner, allowing us to evaluate the performance of our implementation for surface codes of any size. We simulated up to $d = 15$ as this is the upper bound of d possible in the largest FPGA currently available [20].

We also compare the results obtained from the Vivado simulator with those obtained from the FPGA development board for surface code sizes 7 and smaller, to gain confidence in the correctness of the simulator itself.

Noise Model We use the phenomenological noise model [1] that accounts for errors in both data and ancilla qubits. As decoding for X-errors and Z-errors are independent and identical, we only focus on decoding X-errors in the evaluation.

To emulate noise, we independently flip each qubit with a probability of p (the physical error rate) between every two measurement rounds. This is a widely used approach by prior QEC decoders [7, 8, 18]. We then generate the syndrome from the physical errors and provides it as input to our decoder.

For most of our experiments, we use as default $p = 0.001$, like other works [7]. This value is reasonable for surface codes, as p should be sufficiently below the threshold (at least ten times lower) to exponentially reduce errors. We note that the UF decoder has a threshold of $p = 0.026$, calculated by Delfosse and Nickerson [10].

6.2 Decoding Time

We experimentally show how average time for decoding grows with the size of the surface code. Additionally, we show the effect of noise and buffer size on the average time.

Average time To demonstrate the scalability of our algorithm with respect to the size of the surface code, we plot the average time for decoding against the size of the surface code. In Figure 7 (left) the y-axis shows the average FPGA clock cycle count and the x-axis shows the distance (d) of the surface code. We obtained these values from running the distributed UF decoder on the Vivado simulator where each data point represents the average of 1000 trials. We see that for all 3 physical error rates we tested, average decoding time grows sub-linearly with respect to the surface code size, which satisfies the scalability criteria to avoid an exponential backlog. This implies that the average time to decode a measurement round reduces with increasing d as shown in Figure 7 (right).

Distribution of decoding time To understand the growth of decoding time with respect to the code distance, in Figure 8a we plot the distribution of decoding time for different code distances. The y-axis shows the FPGA clock cycle count and the x-axis shows the distance (d) of the surface code. We ran both our test setups for this experiment and the distribution of FPGA clock cycle count for each surface code size is shown in green, while the distribution of clock cycle count on the Vivado simulator is shown in gray. The average cycle count is indicated with \times .

Due to resource limitations on the ZCU106 FPGA, we are unable to run surface codes with $d > 7$ on the FPGA.

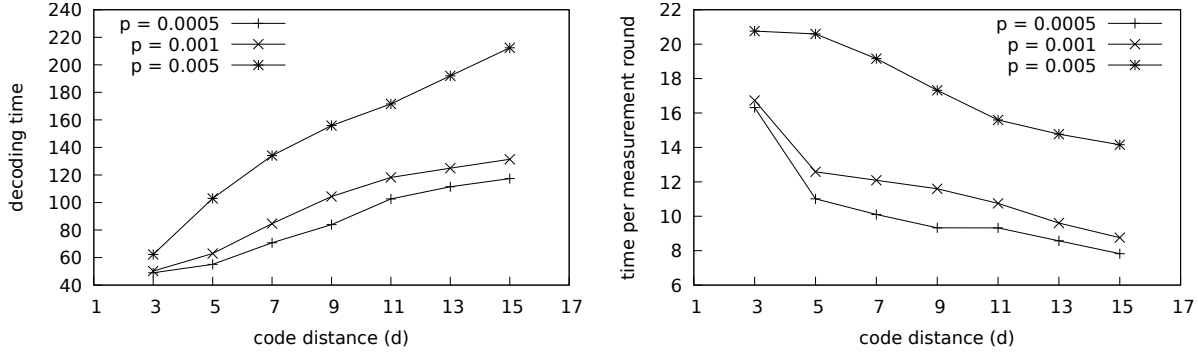


Figure 7: Average decoding time scales sub-linearly with d . We measure the average decoding time for 3 different noise levels using the Vivado simulator. (Left) The average decoding time in FPGA clock cycles. (Right) The average decoding time per measurement round in FPGA clock cycles. Average time per measurement round reducing continuously justifies that our decoder is scalable for large surface codes. We show the distributions separately in [Figure 8a](#)

For $d = 3, 5$ and 7 , the results from the FPGA and those from the Vivado simulator agree. The statistical parameters such as mean, median, and percentile values (P_{25} , P_{75} , P_{90}) differ between running on the FPGA and using the simulator by less than 1%. Only noticeable difference is the higher maximum observed value on the FPGA, which is caused by exponentially unlikely long error chains appearing when running for 10^8 trials in the FPGA. This justifies the use of the Vivado simulator to obtain results for large surface codes that cannot be mapped to the ZCU 106 FPGA board due to resource limitations.

The key factor determining the decoding time is the number of iterations of growing, merging and syncing the distributed UF decoder requires. The peaks in the probability distribution for each distance in [Figure 8a](#) correspond to the number of iterations. The variation around each peak is caused by the delay due to routing messages. The number of iterations is related to the size of the largest cluster, which in turn correlates with the size of the longest error chain in the syndrome. As the size of the surface code increases, the probability of a longer error chain also increases, resulting in the probability distribution shifting to the right.

Furthermore, as seen in [Figure 8a](#), the distribution for each surface code size is right-skewed. For example, for $d = 7$, 90% of trials required two iterations or fewer, which were completed within 140 cycles. In the same test, 99.99% of trials were completed within 237 cycles. Only a very small number of error patterns require long decoding times, corresponding to syndromes with long error chains. Since such syndromes occur rarely and have poor decoding accuracy even if the decoding time is bounded, the impact on accuracy will be minimal.

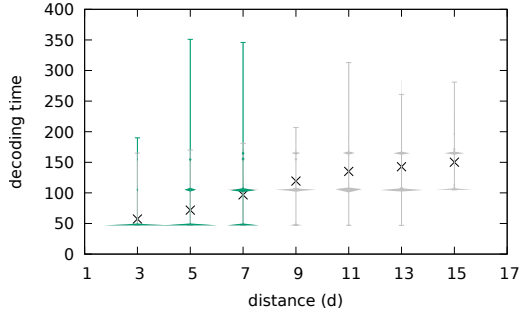
Effect of physical error rate To understand the effect of the physical error rate on decoding time, in [Figure 8b](#) we plot the distribution of latency for three different noise levels. We

obtained this distribution by running on the ZCU106 FPGA with 10^8 trials. The y-axis shows the FPGA clock cycle count and the x-axis shows the physical error rate.

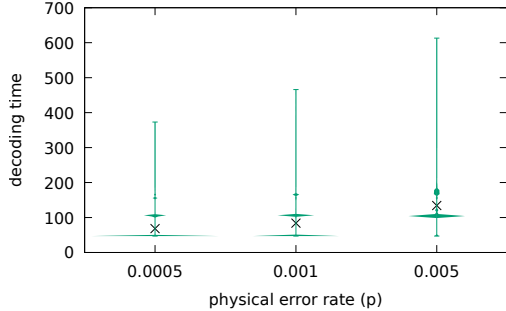
As the noise level increases, the probability distribution of latency shifts to the right. This is caused by the increased probability of a longer error chain when the physical error rate increases, which in turn requires more iterations to decode. As a result, the average decoding time increases with the physical error rate.

Effect of buffer size To measure the impact of the buffer size on decoding time, we varied the buffer size and analyzed the latency distribution. In [Figure 8c](#), the x-axis shows the cycle count and the y-axis shows the cumulative distribution of the latency. We varied the buffer size from 1 to 32. Our results showed that there was no noticeable difference in latency with respect to the buffer size. The obtained results were identical for all buffer sizes above 4 and showed a slowdown of less than 0.01% for buffer sizes of 1 and 2. This indicates that the communication overhead in our design is minimal for the average case

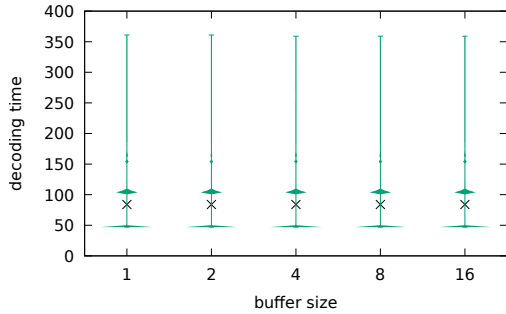
We can explain this result using statistics on the number of messages generated. For example, when the physical error rate is 0.001 and $d = 7$, 97.7% of trials are statistically unaffected by the buffer size. This includes 46% of trials resulting in fully non-trivial syndromes, 47.6% of trials resulting in a single qubit error in each cluster, and 4.1% of trials resulting in a chain of two qubit errors. In all of these cases, at most a single message is generated in each cluster, making the buffer size irrelevant. In the remaining 2.3% of trials, the buffer size will only affect the results if error chains occur close to each other and share a common link in their message paths. In our experiments, such congestion occurred in less than 0.1% of runs. Therefore, the buffer size can be reduced without any significant impact on average decoding time.



(a) Simulator and implementation results agree



(b) Decoding time grows with physical error rate.



(c) Buffer size does not matter for decoding time.

Figure 8: Distribution of decoding time with the average marked with \times . For each error rate we ran 10^8 trials. Results from implementation with Xilinx ZCU 106 FPGA are in green; those from Xilinx Vivado simulator gray. By default $d = 7$, $p = 0.001$.

6.3 Comparison with related work

Our empirical results as shown in Figure 8a suggest that Helios has a lower asymptotic complexity than any existing MWPM or UF implementation for which asymptotic complexities are available, e.g., [10, 17]. Indeed, the empirical results suggest that our decoder has a sub-linear time complexity: the decoding time per round decreases with the number of measurement rounds, which has never been achieved before. This implies that Helios can support arbitrarily large d as rate of decoding will always be faster than the rate of measurement.

Das et al [7] calculate an average latency for their AFS de-

coder based on memory access cycles and assuming a design running at 4 GHz. As the number of memory access cycles grows quadratically with d , the average decoding time per measurement round of AFS grows $O(d^2)$. Similarly, Ueno et al [9] estimate the decoding time of QECOOL from $d = 5$ to $d = 13$ based on SPICE-level simulations with a clock frequency of 5 GHz. For the given range of d the decoding time per measurement round increases quadratically with d . In comparison, the decoding time of Helios decreases per measurement round.

We should like to point out that AFS and QECOOL assume very high clock frequencies, which is key to their estimated low latency. For example, for $d = 11$, AFS and QECOOL respectively report latencies of 42 ns and 8.32 ns per measurement round. Helios, in contrast, requires 107 ns per measurement round with a 100 MHz clock. In terms of clock cycles, Helios requires on average 10.7 cycles for $d = 11$ surface code, lower than both AFS (168 cycles) and QECOOL (41 cycles).

To the best of our knowledge, LILLIPUT [6] is the only hardware decoder in literature that provides implementation-based results, for $d = 5$. The decoder has an average time of 21 ns per measurement round, which is shorter than that of Helios for $d = 5$, i.e., 126 ns. However, as analyzed in §3, LILLIPUT is not scalable for $d > 5$. Our work, in contrast, has successfully demonstrated the implementation of a $d = 7$ surface code on a ZCU106 FPGA with 120 ns per measurement round. The architecture of Helios can potentially support larger d using a larger FPGA, for example $d = 15$ for Xilinx VU19P [20], and even larger d using a network of FPGAs.

7 Conclusion

We describe a distributed design of the Union Find decoder for quantum error-correcting surface codes and present Helios, a system architecture for realizing it. We report an FPGA-based implementation Helios. Using Xilinx Vivado cycle-accurate simulator, we demonstrate empirically that the average decoding time of Helios grows sub-linearly with d . Using a ZCU106 FPGA, we implement the fastest decoding of distance 7 surface codes, which achieves 120ns average decoding time per measurement round. Helios is faster and more scalable than any reported implementation of surface code decoder. Our results suggest that by leveraging parallel hardware resources, Helios can avoid a growing backlog of syndrome measurements for arbitrarily large surface codes.

Acknowledgments

This work was supported in part by Yale University and NSF MRI Award #2216030.

References

- [1] E. Dennis, A. Kitaev, A. Landahl, and J. Preskill, “Topological quantum memory,” *Journal of Mathematical Physics*, vol. 43, no. 9, pp. 4452–4505, 2002.
- [2] A. G. Fowler, M. Mariantoni, J. M. Martinis, and A. N. Cleland, “Surface codes: Towards practical large-scale quantum computation,” *Physical Review A*, vol. 86, no. 3, p. 032324, 2012.
- [3] J. P. Bonilla-Ataides, D. K. Tuckett, S. D. Bartlett, S. T. Flammia, and B. J. Brown, “The XZZX surface code,” *arXiv e-prints*, pp. arXiv–2009, 2020.
- [4] Z. Chen, K. J. Satzinger, J. Atalaya, A. N. Korotkov, A. Dunsworth, D. Sank, C. Quintana, M. McEwen, R. Barends, P. V. Klimov, S. Hong, C. Jones, A. Petukhov, D. Kafri, S. Demura, B. Burkett, C. Gidney, A. G. Fowler, H. Putterman, I. Aleiner, F. Arute, K. Arya, R. Babbush, J. C. Bardin, A. Bengtsson, A. Bourassa, M. Broughton, B. B. Buckley, D. A. Buell, N. Bushnell, B. Chiaro, R. Collins, W. Courtney, A. R. Derk, D. Eppens, C. Erickson, E. Farhi, B. Foxen, M. Giustina, J. A. Gross, M. P. Harrigan, S. D. Harrington, J. Hilton, A. Ho, T. Huang, W. J. Huggins, L. B. Ioffe, S. V. Isakov, E. Jeffrey, Z. Jiang, K. Kechedzhi, S. Kim, F. Kostritsa, D. Landhuis, P. Laptev, E. Lucero, O. Martin, J. R. McClean, T. McCourt, X. Mi, K. C. Miao, M. Mohseni, W. Mruczkiewicz, J. Mutus, O. Naaman, M. Neeley, C. Neill, M. Newman, M. Y. Niu, T. E. O’Brien, A. Opremcak, E. Ostby, B. Pató, N. Redd, P. Roushan, N. C. Rubin, V. Shvarts, D. Strain, M. Szalay, M. D. Trevithick, B. Villalonga, T. White, Z. J. Yao, P. Yeh, A. Zalcman, H. Neven, S. Boixo, V. Smelyanskiy, Y. Chen, A. Megrant, and J. Kelly, “Exponential suppression of bit or phase errors with cyclic error correction,” *Nature*, vol. 595, no. 7867, pp. 383–387, Jul 2021. [Online]. Available: <https://doi.org/10.1038/s41586-021-03588-y>
- [5] C. Gidney and M. Ekerå, “How to factor 2048 bit rsa integers in 8 hours using 20 million noisy qubits,” *Quantum*, vol. 5, p. 433, Apr 2021. [Online]. Available: <http://dx.doi.org/10.22331/q-2021-04-15-433>
- [6] P. Das, A. Locharla, and C. Jones, “LILLIPUT: A lightweight low-latency lookup-table based decoder for near-term quantum error correction,” 2021. [Online]. Available: <https://arxiv.org/abs/2108.06569>
- [7] P. Das, C. A. Pattison, S. Manne, D. Carmean, K. Svore, M. Qureshi, and N. Delfosse, “A scalable decoder micro-architecture for fault-tolerant quantum computing,” *arXiv preprint arXiv:2001.06598*, 2020.
- [8] A. Holmes, M. R. Jokar, G. Pasandi, Y. Ding, M. Pedram, and F. T. Chong, “NISQ+: Boosting quantum computing power by approximating quantum error correction,” 2020. [Online]. Available: <https://arxiv.org/abs/2004.04794>
- [9] Y. Ueno, M. Kondo, M. Tanaka, Y. Suzuki, and Y. Tabuchi, “QECool: On-line quantum error correction with a superconducting decoder for surface code,” in *Proc. ACM/IEEE Design Automation Conference (DAC)*, 2021.
- [10] N. Delfosse and N. H. Nickerson, “Almost-linear time decoding algorithm for topological codes,” *arXiv preprint arXiv:1709.06218*, 2017.
- [11] Xilinx, “Zynq UltraScale+ RFSoc ZCU106 evaluation kit,” <https://www.xilinx.com/products/boards-and-kits/zcu106.html>.
- [12] *Vivado Design Suite User Guide: Logic Simulation*, Xilinx Inc., 04 2022. [Online]. Available: https://www.xilinx.com/content/dam/xilinx/support/documents/sw_manuals/xilinx2022_1/ug900-vivado-logic-simulation.pdf
- [13] Y. Wu, N. Liyanage, and L. Zhong, “An interpretation of union-find decoder on weighted graphs,” 2022. [Online]. Available: <https://arxiv.org/abs/2211.03288>
- [14] B. M. Terhal, “Quantum error correction for quantum memories,” *Reviews of Modern Physics*, vol. 87, no. 2, pp. 307–346, apr 2015. [Online]. Available: <https://doi.org/10.1103/RevModPhys.87.307>
- [15] D. Gottesman, “An introduction to quantum error correction and fault-tolerant quantum computation,” 2009. [Online]. Available: <https://arxiv.org/abs/0904.2557>
- [16] H. Bombín, *Topological codes*. Cambridge University Press, 2013, p. 455–481.
- [17] A. G. Fowler, “Minimum weight perfect matching of fault-tolerant topological quantum error correction in average $O(1)$ parallel time,” 2014.
- [18] L. Skoric, D. E. Browne, K. M. Barnes, N. I. Gillespie, and E. T. Campbell, “Parallel window decoding enables scalable fault tolerant quantum computation,” 2022. [Online]. Available: <https://arxiv.org/abs/2209.08552>
- [19] “Distributed UF on FPGA,” https://github.com/NamiLiy/qec_fpga, 2022.
- [20] Xilinx, “Virtex UltraScale+ VU19P FPGA,” <https://www.xilinx.com/content/dam/xilinx/publications/product-briefs/virtex-ultrascale-plu-s-vu19p-product-brief.pdf>.